International Journal of Medical and Pharmaceutical Sciences
Open access peer-reviewed Journal
Volume 2, Issue 8, Page 246-259.
https://doi.org/10.5281/zenodo.21808205

Research Article

To Design, Develop, and Optimize a Galangin Loaded Thermosensitive In-Situ Nasal Gel for Alzheimer's Disease

Shinde Ramesh*[1], Bade Kanchan[2], Bargaje Goraksh[3]

[1]*Principal of HSBPVT's GOI, Faculty of Pharmacy, Kashti, Maharashtra*
[2]*HOD of Devrao Digamber Varat College of Pharmacy Sakat TQ Jamkhed Dist- Ahilyanagar Maharashtra*
[3]*Principal of Late. Devrao Digamber Varat College of Pharmacy Sakat TQ Jamkhed Dist- Ahilyanagar Maharashtra*

The present study aimed to develop and optimize a galangin-loaded thermosensitive in-situ nasal gel for targeted drug delivery in the treatment of Alzheimer's disease. Galangin, a neuroprotective flavonoid, suffers from poor aqueous solubility and limited bioavailability when administered orally. To overcome these limitations, a nasal in-situ gel formulation was designed using Poloxamer 407 as the thermosensitive polymer and Moringa gum as a mucoadhesive agent. A 3^2 factorial design was employed to optimize two independent variables concentration of Poloxamer 407 and Moringa gum based on the desired responses: gelling temperature and mucoadhesive strength. The optimized batch (F5) showed a gelling temperature of 32.9 °C and mucoadhesive strength of 4562 dynes/cm², closely matching predicted values with relative error <0.5%, validating the statistical model. Physicochemical evaluation demonstrated suitable pH, rapid gelation time, strong gel strength, and temperature-responsive viscosity. FTIR and DSC confirmed the compatibility of galangin with excipients. Ex vivo permeation through goat nasal mucosa exhibited sustained drug release over 12 hours, with F5 achieving 78.46% cumulative permeation. Stability studies confirmed the formulation's robustness under accelerated conditions. The study concludes that the developed in-situ nasal gel offers a promising strategy for enhanced brain delivery of galangin, providing a non-invasive and efficient approach for managing Alzheimer's disease.

Keywords: Galangin; Thermosensitive in-situ gel; Nasal drug delivery; Alzheimer's disease; Poloxamer 407; Moringa gum; Factorial design; Mucoadhesion; Ex vivo permeation; Stability study.

INTRODUCTION

1.1 Overview of Alzheimer's Disease (AD)

Alzheimer's disease (AD) is a chronic, multifactorial, and progressive neurodegenerative disorder that primarily affects the elderly population, leading to a gradual decline in cognitive abilities, functional independence, and overall quality of life. It is clinically classified under the broader category of dementias, representing the most prevalent form, accounting for approximately 60–80% of all dementia cases worldwide. The disease has profound neurological, psychological, social, and economic implications, both for the individuals afflicted and for the global healthcare system. According to the World Health Organization (WHO), Alzheimer's disease is one of the leading causes of disability and dependency among older adults, and its burden is expected to grow exponentially in the coming decades due to increasing life expectancy and demographic transitions. First documented in 1906 by German neuropathologist Dr. Alois Alzheimer, the disease was identified in a 51-year-old patient named Auguste Deter, who exhibited symptoms of profound memory loss, paranoia, language difficulties, and cognitive dysfunction. Post-mortem histopathological examination revealed distinctive changes in the brain, including extracellular amyloid plaques and intracellular neurofibrillary tangles, which have since become

pathognomonic features of the disease. These pathological hallmarks remain at the forefront of current diagnostic and therapeutic research into Alzheimer's disease From a neuropathological standpoint, Alzheimer's disease is characterized by the accumulation of extracellular amyloid-beta (Aβ) plaques and intracellular neurofibrillary tangles (NFTs) composed of hyperphosphorylated tau protein. These features are accompanied by widespread synaptic dysfunction, neuronal loss, neuroinflammation, and cortical atrophy. The hippocampus, a brain region vital for memory formation, is particularly vulnerable in the early stages. Advanced stages involve the parietal and frontal lobes, leading to deficits in language, judgment, and executive function. The clinical diagnosis of Alzheimer's disease is primarily based on comprehensive medical history, caregiver interviews, cognitive assessments, and exclusion of other potential causes of dementia. Tools such as the Mini-Mental State Examination (MMSE), Montreal Cognitive Assessment (MoCA), and neuropsychological batteries help quantify the severity and progression of cognitive decline.

1.2 Epidemiology and Global Burden

Alzheimer's disease (AD) poses a formidable and ever-growing challenge to global public health, with its prevalence and socioeconomic impact expanding dramatically in parallel with the aging global population. As a leading cause of dementia, Alzheimer's disease currently affects more than 55 million people worldwide, and this number is projected to increase to 78 million by 2030 and 139 million by 2050, according to estimates from the World Health Organization (WHO) and Alzheimer's Disease International (ADI). The sheer scale of this neurodegenerative epidemic reflects both advances in longevity and the absence of curative interventions, highlighting a major unmet medical need.

1.3 Etiopathogenesis of Alzheimer's Disease

The etiopathogenesis of Alzheimer's disease (AD) is complex, multifactorial, and not yet fully elucidated, involving a constellation of interrelated biochemical, genetic, molecular, and cellular events that culminate in progressive neurodegeneration. While the hallmark features of the disease extracellular amyloid-β (Aβ) plaques and intracellular neurofibrillary tangles (NFTs) are well-established, recent scientific advances underscore the contribution of multiple overlapping mechanisms including oxidative stress, neuroinflammation, mitochondrial dysfunction, cholinergic deficit, vascular abnormalities, synaptic loss, and genetic predisposition. Understanding these pathogenic pathways is essential not only for accurate diagnosis and staging but also for identifying novel therapeutic targets and optimizing drug delivery strategies aimed at mitigating disease progression [14].

1.4 Tau Protein Hyperphosphorylation and Neurofibrillary Tangles

Another pathological hallmark of AD is the formation of neurofibrillary tangles (NFTs) composed of hyperphosphorylated tau protein, a microtubule-associated protein involved in maintaining axonal integrity and intracellular transport. In AD, tau becomes abnormally phosphorylated, dissociates from microtubules, and aggregates into insoluble paired helical filaments. These tangles accumulate intracellularly, disrupting cytoskeletal structure and neuronal function, ultimately leading to synaptic loss and neuronal death.

1.5 Synaptic Dysfunction and Neurotransmitter Imbalance

Synaptic degeneration is a central feature of Alzheimer's pathology and directly contributes to the deterioration of cognitive and memory functions. Soluble Aβ oligomers are particularly toxic to synapses, impairing long-term potentiation (LTP), reducing dendritic spine density, and disrupting synaptic plasticity.

1.6 Genetic Factors

Genetic predisposition plays a significant role in the development of AD. Early-onset familial AD (EOFAD), though rare, is linked to autosomal dominant mutations in APP, PSEN1, and PSEN2 genes. These mutations typically lead to increased production of Aβ42.

1.7 Vascular Contributions and Blood-Brain Barrier Dysfunction

Increasing evidence suggests that cerebrovascular dysfunction and blood-brain barrier (BBB) disruption significantly contribute to the pathogenesis of AD. Vascular risk factors such as hypertension, diabetes mellitus, hyperlipidemia, and atherosclerosis not only impair cerebral perfusion but also exacerbate amyloid accumulation by compromising Aβ clearance across the BBB.

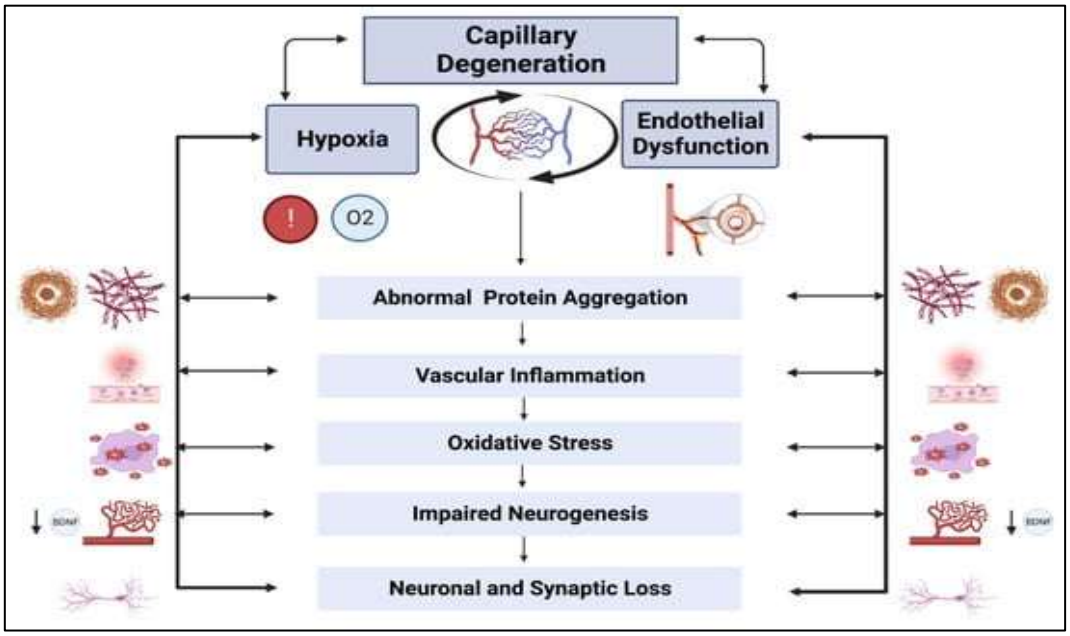

Figure 1.1: Pathogenesis of Alzheimer's disease.

1.8 Nasal Drug Delivery: A Platform for Brain Targeting

The nasal cavity is a highly vascularized and functionally dynamic anatomical structure that serves not only as the primary entryway for inhaled air but also as an increasingly recognized route for drug delivery, particularly for targeting the central nervous system. Anatomically, the nasal cavity is divided into two symmetrical halves by the nasal septum, each containing three distinct regions: the vestibular, respiratory, and olfactory regions. Each of these subregions plays a unique role in filtration, humidification, immune defense, and drug absorption, making the nasal cavity a sophisticated and multifaceted interface between the external environment and internal physiological systems [30].

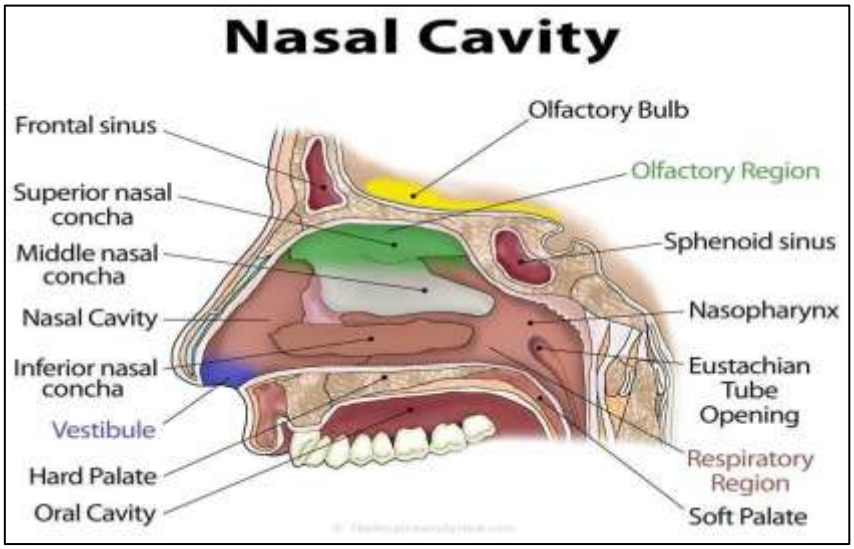

Figure 1.2: Anatomy of nasal cavity

2. Drug and Excipient Profile

2.1. Drug Profile

Galangin [68]	
Synonym	3,5,7-Trihydroxyflavone
Background	Galangin is a natural flavonoid primarily found in *Alpinia officinarum* (lesser galangal) and *Helichrysum aureonitens*. It has potent antioxidant, anti-inflammatory, antimicrobial, and neuroprotective activities, making it a promising compound for neurodegenerative disorders.
CAS Registry Number	548-83-4
IUPAC Name	3,5,7-Trihydroxy-2-phenyl-4H-1-benzopyran-4-one
Description	Galangin is a yellow crystalline solid flavonoid compound belonging to the flavonol subclass, known for its polyphenolic structure and bioactivity.
Molecular Formula	$C_{15}H_{10}O_5$
Molecular Weight	270.24 g/mol
Chemical Structure	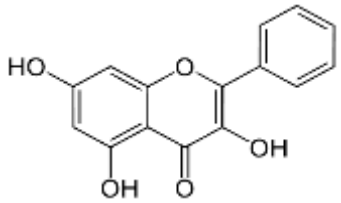
Solubility	Practically insoluble in water; soluble in ethanol, methanol, and DMSO
pH	Neutral compound; stable in pH range 5–7
Melting Point	315–317°C
Handling Precautions	Use in a well-ventilated area; avoid inhalation and contact with skin and eyes; wear gloves and protective clothing
Pharmacology	Exhibits neuroprotective, anti-amyloid, antioxidant, anti-inflammatory, antibacterial, anticancer, and hepatoprotective effects
Pharmacodynamics	Galangin modulates multiple molecular pathways including reduction of ROS, inhibition of pro-inflammatory cytokines, and suppression of Aβ aggregation
Mechanism of Action	Galangin exerts its neuroprotective effect by inhibiting amyloid beta-induced toxicity, downregulating pro-inflammatory mediators, scavenging free radicals, and modulating signaling pathways such as NF-κB and MAPK
Metabolism	Undergoes phase II metabolism via glucuronidation and sulfation in the liver
Elimination	Primarily excreted via feces and urine as conjugated metabolites
Functional Category	Natural flavonoid; Antioxidant; Anti-inflammatory; Neuroprotective agent
Stability and Storage Conditions	Store in a cool, dry place away from light and moisture; stable under standard laboratory conditions
Incompatibilities	Incompatible with strong oxidizing agents and strong acids
Applications	Investigated for treatment in Alzheimer's disease, cancer, microbial infections, liver disorders, and inflammatory conditions
Adverse Effects	Generally considered safe at lower concentrations; high doses may cause gastrointestinal irritation or hepatotoxicity in animal studies
Safety	GRAS (Generally Recognized As Safe) status not yet officially designated; use under experimental and controlled conditions

MATERIALS AND METHODS

3.1. MATERIALS

Table 3.1.1: List of Materials used.

Sr. No	Materials	Source
1	Gelangin	Sciquaint Innovations Pvt. Ltd., Pune, India
2	Poloxamer 407	BASF India Ltd., Mumbai, India
3	Moringa gum	Extracted and purified in-house
4	Disodium EDTA	Loba Chemie Pvt. Ltd., Mumbai, India

5	Benzalkonium chloride	Loba Chemie Pvt. Ltd., Mumbai, India
6	Propylene glycol	SD Fine Chemicals Ltd., Mumbai, India
7	Potassium dihydrogen phosphate	Merck Specialities Pvt. Ltd., Mumbai, India
8	Sodium hydroxide	Merck Specialities Pvt. Ltd., Mumbai, India
9	Potassium bromide (KBr)	Sigma-Aldrich, India

Table 3.1.2: List of Equipment's used

Sr. No.	Instrument	Company
1	Digital weighing balance	Shimadzu AUX220
2	Hot air oven	York Scientific industries Pvt. Ltd.
8	UV-Visible Spectrophotometer	Shimadzu UV1800
9	Fourier Transform Infrared Spectrophotometer	Shimadzu 1800
10	Franz diffusion cell apparatus	Pharmagel Engineering SPA
11	Differential scanning colorimetry (DSC)	MicroCal Analyzer
12	Water bath (electronic)	Labline stock centre
13	Digital pH meter	Mettler Toledo
14	Brookfield Viscometer	Ametek
15	Incubator	-
16	Centrifuge machine	Doctors Centrifuge

METHODS

3.2.1. UV-Visible Spectroscopy and Calibration Curve of Galangin

The UV-Visible spectrophotometric analysis of galangin was carried out to determine its wavelength of maximum absorption (λmax), which is essential for its quantitative estimation. Due to galangin's poor aqueous solubility, a stock solution was prepared by dissolving 1 mg/mL of galangin in methanol. The solution was scanned over the wavelength range of 200–400 nm using a double-beam UV-Visible spectrophotometer (Shimadzu UV-1800, Shimadzu India Analytical Instruments Pvt. Ltd., Mumbai, India). The absorption maximum (λmax) was observed at 360 nm and was selected for all subsequent quantitative analyses. For the preparation of the calibration curve, a series of standard solutions of galangin were prepared from the stock solution at concentrations of 5, 10, 15, 20, 25, and 30 µg/mL in methanol. The absorbance of each solution was measured at 360 nm against methanol as the blank. All measurements were performed in triplicate (n=3) to ensure accuracy and reproducibility. A calibration curve was then constructed by plotting the mean absorbance values against their respective concentrations. Linear regression analysis was performed, and the resulting equation was used for further quantification of galangin in formulation studies [72].

3.2.2. Fourier Transform Infrared (FTIR) Spectroscopy Analysis

FTIR spectroscopy was carried out to assess potential drug–excipient interactions between galangin and individual formulation components. FTIR spectra were recorded for pure galangin, individual excipients, and physical mixtures of galangin with each excipient in a 1:1 (w/w) ratio. The analysis was performed using an FTIR spectrophotometer (Bruker Alpha II, Bruker India Scientific Pvt. Ltd., Mumbai, India). Approximately 2–3 mg of each sample was finely ground and mixed with potassium bromide (KBr) at a ratio of 1:100 (sample:KBr) and compressed into translucent pellets using a hydraulic press under 10 tons of pressure for 5 minutes. Spectral data were collected in the range of 4000 to 400 cm^{-1} at a resolution of 4 cm^{-1} with 32 scans per sample. The characteristic peaks of galangin and excipients were analyzed and compared with those of the physical mixtures to identify any potential chemical interactions. All measurements were conducted at room temperature (25 ± 2°C), and each sample was evaluated in triplicate (n = 3) [73,74].

3.2.3. Differential Scanning Calorimetry (DSC) Analysis

Differential Scanning Calorimetry (DSC) analysis was conducted to evaluate the thermal behavior of galangin, individual excipients, and their physical mixtures, and to identify any possible drug–excipient interactions. The analysis was performed using a DSC instrument (Mettler Toledo DSC 3+, Mettler Toledo India Pvt. Ltd., Mumbai, India) equipped with a refrigerated cooling system. Approximately 2–5 mg of each accurately weighed sample was sealed in an aluminum pan, while an empty sealed pan was used as the reference. The samples were scanned over a temperature range of 30°C to 300°C at a constant heating rate of 10°C/min under a dynamic nitrogen atmosphere with a flow rate of 40 mL/min to prevent oxidative degradation. The thermograms obtained for pure drug, individual excipients, and physical mixtures (1:1 w/w) were compared to assess any changes in the onset temperature, melting point, peak shape, or enthalpy that might indicate potential physical or chemical interactions. Each sample was analyzed in triplicate to ensure reproducibility, and the analysis was performed under controlled laboratory conditions at ambient temperature (25 ± 2°C) [75].

3.2.4 Experimental Design for Formulations

A 3^2 full factorial design was employed to optimize the formulation of galangin-loaded thermosensitive in-situ nasal gel. Two independent formulation variables were selected: the concentration of Poloxamer 407 (X_1), serving as the thermogelling polymer, and the concentration of mucoadhesive polymer (X_2). Each variable was studied at three levels: low (-1), medium (0), and high (+1). The chosen dependent variables were gelling temperature (Y_1) and mucoadhesive strength (Y_2), as these are critical quality attributes influencing nasal retention and therapeutic efficacy. A total of nine experimental batches were prepared based on the design matrix, each representing a unique combination of the two independent variables. The design aimed to evaluate both the main and interaction effects of the variables on the formulation's performance. The relationship between the independent and dependent variables was expressed by the following second-order polynomial equation.

Table 3.3: Variables in 3^2 Factorial Design

Independent Variables	Levels		
	Low (-1)	Medium (0)	High (+1)
X_1: Poloxamer 407 (% w/v)	16	18	20
X_2: Moringa gum (% w/v)	0.5	1.0	1.5
Dependent Variables			**Goal**
Y_1: Gelling Temperature (°C)			30-34
Y_2: Mucoadhesive Strength			Maximize

Table 3.4: Composition of Galangin-loaded Thermosensitive In-situ Nasal Gel Formulations

Ingredients (% w/v)	F1	F2	F3	F4	F5	F6	F7	F8	F9
Galangin	0.05	0.05	0.05	0.05	0.05	0.05	0.05	0.05	0.05
Poloxamer 407	16	16	16	18	18	18	20	20	20
Moringa gum	0.3	0.5	0.7	0.3	0.5	0.7	0.3	0.5	0.7
Benzalkonium chloride	0.01	0.01	0.01	0.01	0.01	0.01	0.01	0.01	0.01
Disodium EDTA	0.05	0.05	0.05	0.05	0.05	0.05	0.05	0.05	0.05
Propylene glycol	10.0	10.0	10.0	10.0	10.0	10.0	10.0	10.0	10.0
Phosphate buffer (pH 6.4)	q.s.	q.s.	q.s.	q.s.	q.s.	q.s.	q.s.	q.s.	q.s.

3.2.5. Preparation of Galangin-loaded Thermosensitive In-situ Nasal Gel

The thermosensitive in-situ nasal gels were prepared using the cold method as described by Schmolka with modifications suitable for galangin incorporation. Briefly, Poloxamer 407 (thermogelling agent) was slowly added to cold phosphate buffer (pH 6.4, 5°C) under continuous magnetic stirring at 400 rpm. The

dispersion was refrigerated at 4°C for 24 hours to ensure complete hydration of the polymer. Moringa gum (mucoadhesive agent) was separately dissolved in 1% v/v glacial acetic acid solution and neutralized with sodium hydroxide to achieve pH 6.4, then mixed with phosphate buffer at room temperature with constant stirring at 500 rpm for 2 hours. Benzalkonium chloride (0.01% w/v) and disodium EDTA (0.05% w/v) were added as preservative and chelating agent, respectively. Galangin (0.05% w/v) was dissolved in propylene glycol (10% v/v) with sonication for 15 minutes to ensure complete dissolution and added to the Poloxamer solution under constant stirring at 4°C. Finally, the chitosan solution was gradually added to the Poloxamer-galangin solution with gentle stirring to avoid air entrapment. The volume was adjusted with phosphate buffer (pH 6.4), and the formulation was stored at 4°C for further studies. Nine different formulations (F1-F9) were prepared according to the experimental design, with varying concentrations of Poloxamer 407 and chitosan, as shown in Table 7.4 [80].

RESULTS AND DISCUSSION

4.1. RESULTS

4.1.1. Organoleptic evaluation of pure drug

The organoleptic evaluation of pure galangin confirmed its conformity with standard pharmacognostic attributes.

Table 4.1: Organoleptic Evaluation of Pure Galangin

Sr. No.	Parameter	Observed	Standard
1	Color	Yellow crystalline powder	Yellow crystalline powder
2	Odor	Odorless	Odorless
3	Texture	Fine powder	Fine powder

4.1.2. Scanning absorbance maxima

The organoleptic assessment of pure galangin confirmed its compliance with standard reference characteristics. As shown in Table: *Organoleptic Evaluation of Pure Galangin*, the substance appeared as a yellow crystalline powder, which aligns with literature-reported physical descriptions. The absence of odor and the presence of a fine powder texture further validate the compound's identity and purity. These physical properties are critical in preliminary evaluations for confirming drug authenticity and suitability for formulation development. The UV-Visible spectroscopic analysis revealed that galangin exhibited a strong absorption maximum (λmax) at 268 nm, as illustrated in the respective figure. This absorbance peak corresponds to the characteristic electronic transitions of flavonol compounds, confirming the presence of conjugated aromatic systems in galangin. This λmax value is critical for further analytical quantification, particularly in drug content and solubility determination. The sharp and defined peak supports the chemical purity and electronic configuration expected for galangin.

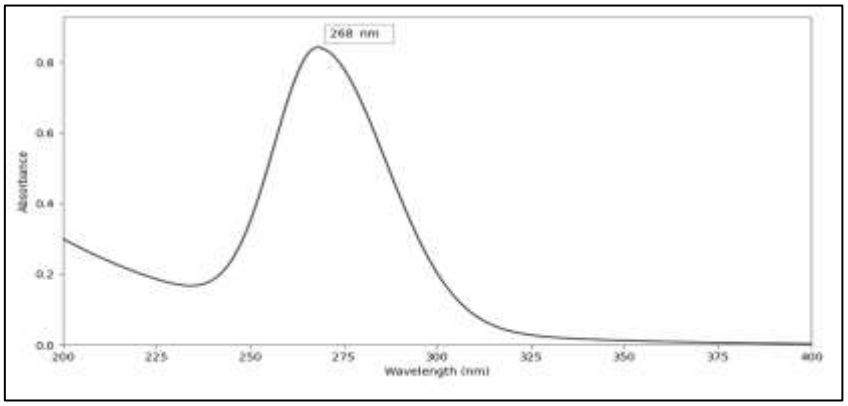

Figure 4.1: Scanning absorbance maxima of galangin (268 nm)

4.1.3. Calibration curve determination

The calibration curve of galangin in methanol exhibited excellent linearity across the tested concentration range of 5 to 30 µg/mL, with a correlation coefficient (R^2) of 0.9999. The absorbance values increased proportionally with concentration, confirming the method's suitability for quantitative analysis. The slope and intercept of the curve were 0.0285 and 0.0013, respectively, and the absorbance maximum was observed at 268 nm. These findings indicate a reliable and precise UV-visible spectrophotometric method for determining galangin concentration.

Table 4.2

Sr. No.	Concentration (µg/mL)	Absorbance (Mean ± SD)
1	5	0.142 ± 0.003
2	10	0.287 ± 0.004
3	15	0.430 ± 0.005
4	20	0.571 ± 0.006
5	25	0.712 ± 0.004
6	30	0.854 ± 0.005
Slope		0.0285
Intercept		0.0013
R^2		0.9999
Absorption maxima		268nm

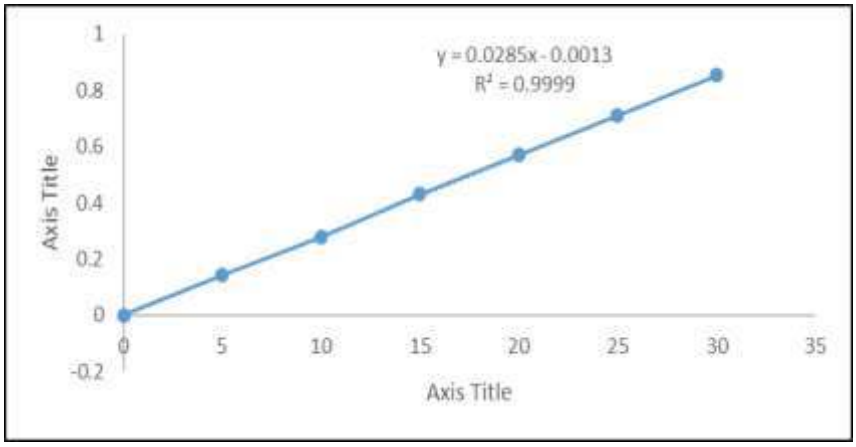

Figure 4.2: Calibration curve of galangin in methanol

4.1.4. Solubility study

Table 4.3: Solubility Profile of Galangin in Various Solvents

Sr. No.	Solvent	Solubility (mg/mL) (Mean ± SD)	Inference (USP Descriptive Term)
1	Ethanol	29.85 ± 0.52	Soluble (s)
2	Methanol	30.12 ± 0.47	Soluble (s)
3	Distilled Water	0.008 ± 0.002	Practically insoluble (pi)
4	Phosphate buffer (pH 7.2)	0.26 ± 0.01	Sparingly soluble (sps)
5	DMSO	52.43 ± 1.18	Freely soluble (fs)

All values are expressed as mean ± SD.

4.1.5. Melting point determination

The solubility study of galangin revealed significant variation across different solvents. It was found to be soluble in ethanol (29.85 ± 0.52 mg/mL) and

methanol (30.12 ± 0.47 mg/mL), and freely soluble in DMSO (52.43 ± 1.18 mg/mL), indicating high affinity in organic solvents. In contrast, galangin was practically insoluble in distilled water (0.008 ± 0.002 mg/mL) and sparingly soluble in phosphate buffer pH 7.2 (0.26 ± 0.01 mg/mL), confirming its poor aqueous solubility. These findings support the need for formulation strategies to enhance galangin's solubility and bioavailability.

Table 4.4: Melting Point Determination of Galangin

Sr. No.	Melting Point Observed (°C)	Standard Melting Point (°C)
1	214.6 ± 0.5	214–215

4.1.6. Differential scanning colorimetry (DSC)

The DSC thermogram of pure galangin exhibited a sharp endothermic peak at 214.94 °C, corresponding to its melting point, indicating its crystalline nature. In contrast, the DSC thermogram of the physical mixture showed two distinct endothermic peaks at 71.79 °C and 214.45 °C. The appearance of the galangin peak near its original melting point in the mixture confirms the absence of significant interaction with excipients, while the additional lower temperature peak likely represents the melting or thermal transition of one of the excipients.

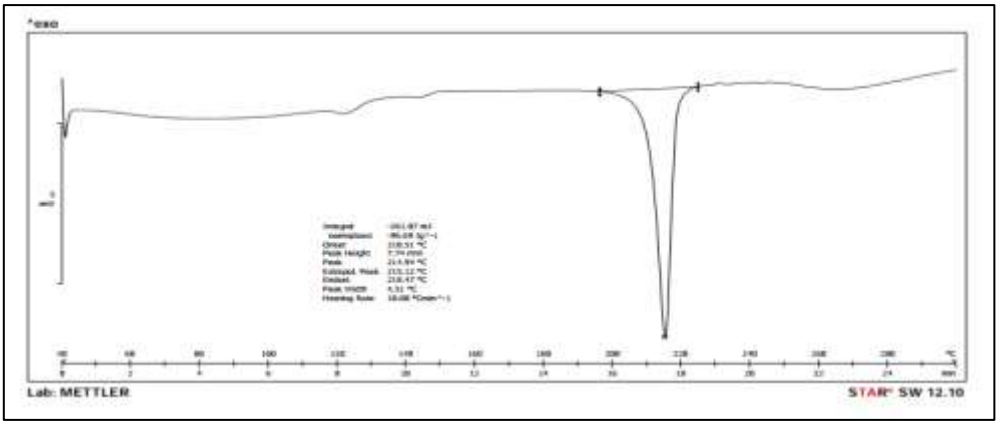

Figure 4.3: DSC spectra of pure galangin

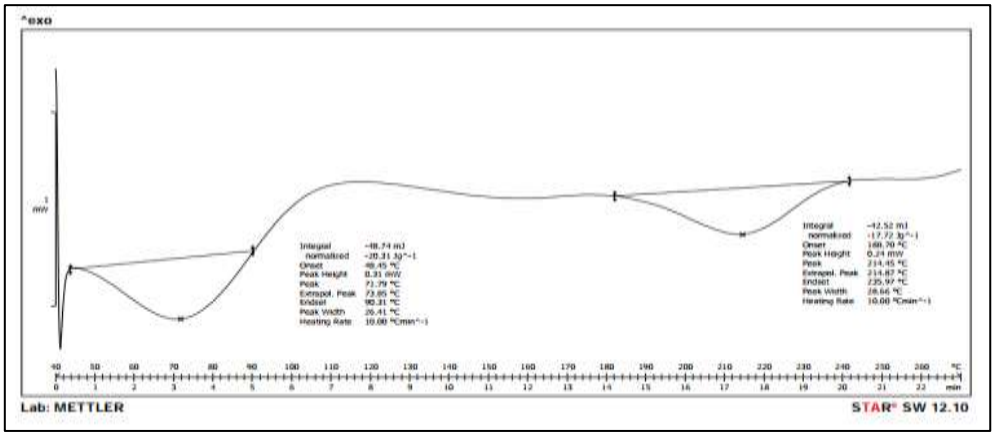

Figure 4.4: DSC spectra of physical mixture (Drug + Excipients)

4.1.7. FTIR spectroscopy

The FTIR spectra of pure galangin confirmed the presence of characteristic functional groups, with a prominent O–H stretching vibration at 3321.34 cm^{-1}, and alkyl C–H stretching bands at 2944.19 and 2832.40 cm^{-1}. The C=C aromatic stretch appeared at 1449.10 cm^{-1}, while the phenolic C–O stretch was

observed at 1020.69 cm^{-1}. In the physical mixture, similar peaks were retained with slight shifts, such as O–H at 3374.09 cm^{-1} and C–H stretching at 2873.15 cm^{-1}, indicating no significant chemical interaction between the drug and excipients.

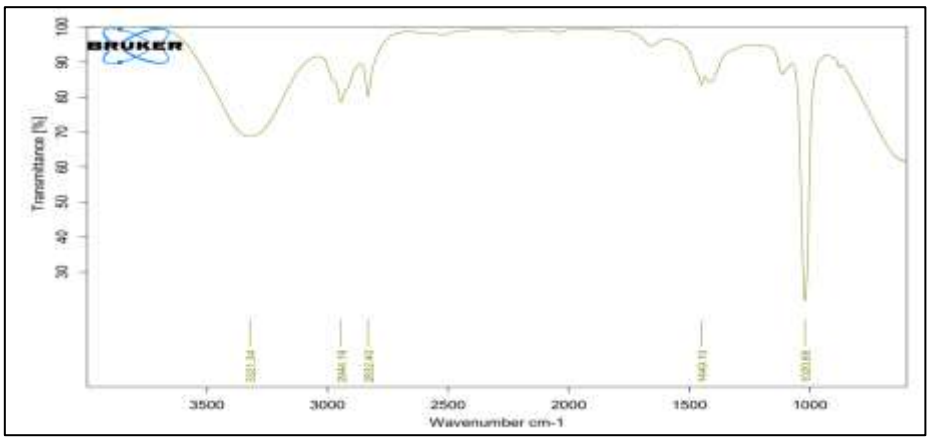

Figure 4.5: FTIR spectra of pure drug

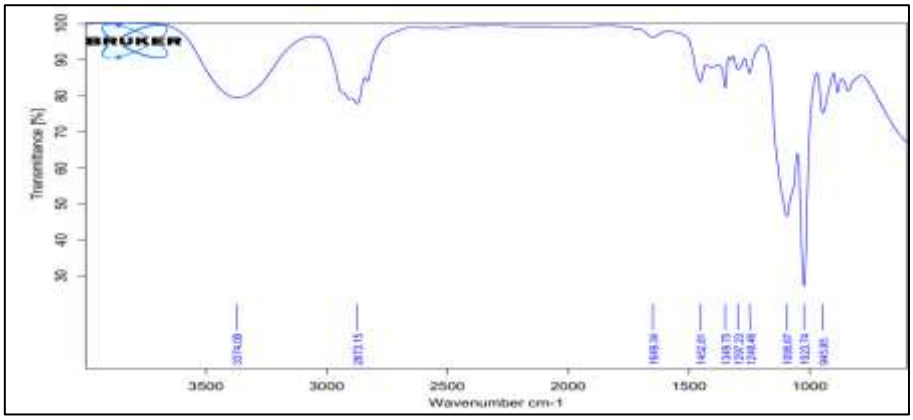

Figure 4.6: FTIR spectra of physical mixture.

Table 4.5: FTIR Interpretation

Functional Group	Standard Wavelength Range (cm^{-1})	Observed in Pure Drug (cm^{-1})	Observed in Physical Mixture (cm^{-1})
O–H Stretch (Phenolic)	3200–3600	3321.34	3374.09
C–H Stretch (Alkyl)	2850–2960	2944.19, 2832.40	2873.15
C=C Aromatic Stretch	1400–1600	1449.10	1452.81, 1649.34
C–O Stretch (Phenolic)	1000–1300	1020.69	1023.74, 1095.67
C–C Stretch / C–O–C	1200–1300	—	1249.46, 1297.23, 1294.46
C–H Bending (Aromatic)	~900–1000	—	945.95

4.1.8. Characterization of Galangin-Loaded Thermosensitive In-Situ Nasal Gel

All formulations (F1 to F9) of the galangin-loaded thermosensitive in-situ nasal gel exhibited a consistent pale yellow, transparent appearance with clear clarity and no visible particulate matter. This uniform visual profile across batches confirms successful incorporation of galangin without affecting the physical integrity or aesthetic quality of the gel formulations.

Table 4.6: Visual Assessment of Galangin-Loaded Thermosensitive In-Situ Nasal Gel Formulations

F. Code	Physical Appearance	Clarity	Particulate Matter
F1	Pale yellow, transparent	Clear	Absent
F2	Pale yellow, transparent	Clear	Absent
F3	Pale yellow, transparent	Clear	Absent
F4	Pale yellow, transparent	Clear	Absent
F5	Pale yellow, transparent	Clear	Absent
F6	Pale yellow, transparent	Clear	Absent
F7	Pale yellow, transparent	Clear	Absent
F8	Pale yellow, transparent	Clear	Absent
F9	Pale yellow, transparent	Clear	Absent

The physicochemical evaluation of galangin-loaded thermosensitive in-situ nasal gel formulations (F1–F9) revealed pH values ranging from 6.21 to 6.33, which are within the acceptable nasal tolerance range. Gelation time decreased progressively from F1 (59.1 sec) to F9 (31.0 sec), indicating improved thermoresponsive behavior with increasing polymer concentration. Gel strength showed a corresponding increase, with F1 exhibiting 24.3 g and F9 reaching 46.1 g, suggesting enhanced structural integrity. The viscosity at 4°C and 34°C increased steadily across formulations, with F1 showing 553 cP and 5798 cP, while F9 recorded 1136 cP and 9112 cP, respectively, reflecting greater thermal responsiveness. Drug content remained consistently high (97.58%–99.18%), demonstrating efficient drug incorporation and uniformity across batches.

Table 4.7: Critical Physicochemical Parameters of Galangin-Loaded Thermosensitive In-Situ Nasal Gel Formulations

F. Code	pH	Gelation Time (sec)	Gel Strength (g)	Viscosity at 4°C (cP)	Viscosity at 34°C (cP)	Drug Content (%)
F1	6.33 ± 0.05	59.1 ± 2.4	24.3 ± 1.4	553 ± 21	5798 ± 138	98.31 ± 1.02
F2	6.29 ± 0.04	55.3 ± 3.0	27.0 ± 1.3	619 ± 26	5992 ± 149	97.94 ± 1.15
F3	6.26 ± 0.03	51.7 ± 2.6	31.6 ± 1.5	678 ± 29	6255 ± 173	96.89 ± 1.41
F4	6.31 ± 0.05	47.1 ± 2.1	33.6 ± 1.3	739 ± 25	7010 ± 161	99.18 ± 0.90
F5	6.28 ± 0.04	44.6 ± 2.4	36.5 ± 1.7	785 ± 31	7295 ± 177	98.52 ± 1.08
F6	6.25 ± 0.05	42.1 ± 2.5	40.6 ± 1.6	866 ± 36	7618 ± 191	97.87 ± 1.27
F7	6.30 ± 0.03	35.1 ± 2.0	39.7 ± 1.6	958 ± 41	8355 ± 206	99.09 ± 0.92
F8	6.26 ± 0.04	33.3 ± 2.2	43.2 ± 1.9	1051 ± 44	8728 ± 213	98.41 ± 1.14
F9	6.21 ± 0.05	31.0 ± 2.1	46.1 ± 2.1	1136 ± 52	9112 ± 223	97.58 ± 1.33

Values represent mean ± SD (n = 3).

The rheological and adhesive evaluation of galangin-loaded thermosensitive in-situ nasal gel formulations (F1–F9) indicated a consistent increase in mucoadhesive strength from 3289 dynes/cm² in F1 to 5067 dynes/cm² in F9, demonstrating the enhanced bioadhesion due to increasing polymer concentration. Gelation temperature showed a gradual decrease across batches, ranging from 35.8 °C in F1 to 29.7 °C in F9, signifying improved thermosensitivity. Correspondingly, spreadability values decreased from 24.2 g·cm/s (F1) to 13.0 g·cm/s (F9), indicating reduced flowability with enhanced structural rigidity, which supports better nasal retention. These results affirm the desired correlation between formulation composition and functional performance.

Table 4.8: Rheological and Adhesive Properties of Galangin-Loaded Thermosensitive In-Situ Nasal Gel Formulations

Formulation	Mucoadhesive Strength (dynes/cm²)	Gelation Temperature (°C)	Spreadability (g·cm/s)
F1	3289 ± 135	35.8 ± 0.7	24.2 ± 1.3
F2	4170 ± 159	35.2 ± 0.6	22.1 ± 1.0
F3	4408 ± 178	34.7 ± 0.8	20.1 ± 1.2
F4	3495 ± 148	33.4 ± 0.5	21.2 ± 1.1
F5	4562 ± 165	32.9 ± 0.6	19.0 ± 1.3
F6	4824 ± 192	32.3 ± 0.7	16.2 ± 1.0
F7	3647 ± 153	30.5 ± 0.6	18.1 ± 1.1
F8	4748 ± 189	30.1 ± 0.4	15.3 ± 1.0
F9	5067 ± 207	29.7 ± 0.5	13.0 ± 1.2

Values represent mean ± SD (n = 3).

5. SUMMARY AND CONCLUSION

5.1. SUMMARY

The present research aimed at developing a novel thermosensitive in-situ nasal gel system for the delivery of galangin, a bioactive flavonoid with neuroprotective potential, for the treatment of Alzheimer's disease. Galangin's limited aqueous solubility and poor brain bioavailability through conventional routes necessitated the design of a nasal delivery system to enhance brain targeting via the olfactory pathway. The formulation strategy incorporated Poloxamer 407 as a thermoresponsive gelling polymer and Moringa gum as a natural mucoadhesive agent. Preformulation studies including organoleptic assessment, solubility profiling, FTIR, and DSC confirmed the purity of the drug and its compatibility with excipients. A 3^2 factorial design was used to evaluate the impact of polymer concentrations on gelling temperature and mucoadhesive strength. Nine batches were prepared and assessed for visual appearance, pH, gelation time, gel strength, viscosity, drug content, rheology, and mucoadhesive properties. Ex vivo permeation studies using goat nasal mucosa revealed controlled and sustained drug permeation, with formulation F5 showing optimal results. Statistical analysis showed that the quadratic model was significant ($p < 0.05$) with high R^2 values (>0.99), indicating a strong fit. The optimized batch (F5) exhibited a gelling temperature of 32.9 °C and mucoadhesive strength of 4562 dynes/cm², closely matching predicted values with minimal error. Accelerated stability studies confirmed the formulation's stability over 3 months under ICH conditions.

CONCLUSION

The present study comprehensively addressed the formulation challenges associated with the nasal delivery of galangin, a flavonoid with proven neuroprotective potential, for the treatment of Alzheimer's disease. By leveraging the advantages of thermosensitive in-situ gel systems, this research successfully designed and optimized a novel nasal drug delivery system capable of enhancing galangin's therapeutic efficacy and targeting the brain more effectively via the olfactory route. The use of Poloxamer 407 provided the necessary thermogelling properties, enabling the formulation to remain in a liquid state at room temperature and transition into a gel at physiological nasal temperature, ensuring prolonged mucosal contact. Additionally, the incorporation of Moringa gum imparted mucoadhesive strength, enhancing the formulation's retention time and bioavailability. Through systematic experimentation using a 3^2 factorial design, critical formulation variables were optimized to achieve ideal gelling temperature and mucoadhesive strength. Statistical analysis validated the significance of the quadratic model with high adjusted and predicted R^2 values, and polynomial equations successfully predicted the behavior of responses. The optimized batch (F5) exhibited a gelling temperature of 32.9 °C and a mucoadhesive strength of 4562 dynes/cm², closely matching the predicted values with a relative error below 0.5%,

confirming the reliability of the model. The formulation displayed acceptable physicochemical characteristics including suitable pH, gelation time, gel strength, and excellent drug content uniformity. Viscosity measurements confirmed low viscosity at storage temperature and high viscosity upon gelation, validating temperature-responsive behavior. FTIR and DSC analyses confirmed drug-excipient compatibility and absence of physical or chemical interactions. Ex vivo permeation studies demonstrated sustained release of galangin over 12 hours, with F5 exhibiting superior permeation performance, indicative of its potential for prolonged therapeutic action. Furthermore, accelerated stability testing showed minimal degradation and no significant changes in performance attributes, confirming the formulation's robustness over time.

REFERENCES

1. Moloney CM, Labuzan SA, Crook JE, Siddiqui H, Castillo-Carranza DL, Sengupta U, et al. Visualization of neurofibrillary tangle maturity in Alzheimer's disease: A clinicopathologic perspective for biomarker research. Alzheimers Dement. 2021;17(9):1554-1574. doi:10.1002/alz.12321
2. Ward A, Tardiff S, Dye C, Arrighi HM. Rate of conversion from prodromal Alzheimer's disease to Alzheimer's dementia: a systematic review of the literature. Dement Geriatr Cogn Dis Extra. 2013;3(1):320-332. doi:10.1159/000354370
3. Petersen RC, Doody R, Kurz A, Mohs RC, Morris JC, Rabins PV, et al. Current concepts in mild cognitive impairment. Arch Neurol. 2001;58(12):1985-1992. doi:10.1001/archneur.58.12.1985
4. Burns A, Iliffe S. Alzheimer's disease. BMJ. 2009;338: b158. doi:10.1136/bmj. b158
5. Selkoe DJ. Alzheimer's disease is a synaptic failure. Science. 2002;298(5594):789-791. doi:10.1126/science.1074069
6. Kumar A, Singh A, Ekavali. A review on Alzheimer's disease pathophysiology and its management: an update. Pharmacol Rep. 2015;67(2):195-203. doi: 10.1016/j.pharep.2014.09.004
7. Cummings J, Lee G, Ritter A, Sabbagh M, Zhong K. Alzheimer's disease drug development pipeline: 2019. Alzheimers Dement (N Y). 2019; 5:272-293. doi: 10.1016/j.trci.2019.05.008
8. GBD 2019 Dementia Forecasting Collaborators. Estimation of the global prevalence of dementia in 2019 and forecasted prevalence in 2050: an analysis for the Global Burden of Disease Study 2019. Lancet Public Health. 2022;7(2):e105-e125. doi:10.1016/S2468-2667(21)00249-8
9. Prince M, Wimo A, Guerchet M, Ali GC, Wu YT, Prina M. World Alzheimer Report 2015 - The Global Impact of Dementia: An analysis of prevalence, incidence, cost and trends. London: Alzheimer's Disease International; 2015.
10. Wimo A, Seeher K, Cataldi R, Cyhlarova E, Dielemann JL, Frisell O, et al. The worldwide costs of dementia in 2019. Alzheimers Dement. 2023;19(7):2865-2873. doi:10.1002/alz.12901
11. [11] Jia L, Du Y, Chu L, Zhang Z, Li F, Lyu D, et al. Prevalence, risk factors, and management of dementia and mild cognitive impairment in adults aged 60 years or older in China: a cross-sectional study. Lancet Public Health. 2020;5(12):e661-e671. doi:10.1016/S2468-2667(20)30185-7
12. WHO. Global action plan on the public health response to dementia 2017-2025. Geneva: World Health Organization; 2017.
13. Gauthier S, Rosa-Neto P, Morais JA, Webster C. World Alzheimer Report 2021: Journey through the diagnosis of dementia. London: Alzheimer's Disease International; 2021.
14. Hardy J, Selkoe DJ. The amyloid hypothesis of Alzheimer's disease: progress and problems on the road to therapeutics. Science. 2002;297(5580):353-356. doi:10.1126/science.1072994
15. Braak H, Braak E. Neuropathological stageing of Alzheimer-related changes. Acta Neuropathol. 1991;82(4):239-259. doi:10.1007/BF00308809
16. Butterfield DA, Halliwell B. Oxidative stress, dysfunctional glucose metabolism and Alzheimer disease. Nat Rev Neurosci. 2019;20(3):148-160. doi:10.1038/s41583-019-0132-6
17. Heneka MT, Carson MJ, El Khoury J, Landreth GE, Brosseron F, Feinstein DL, et al. Neuroinflammation in Alzheimer's disease. Lancet Neurol. 2015;14(4):388-405. doi:10.1016/S1474-4422(15)70016-5
18. Mancuso C, Santangelo R. Alzheimer's disease and gut microbiota modifications: The long way

between preclinical studies and clinical evidence. Pharmacol Res. 2018; 129:329-336. doi: 10.1016/j.phrs.2017.12.009
19. Dubois B, Feldman HH, Jacova C, Hampel H, Molinuevo JL, Blennow K, et al. Advancing research diagnostic criteria for Alzheimer's disease: the IWG-2 criteria. Lancet Neurol. 2014;13(6):614-629. doi:10.1016/S1474-4422(14)70090-0
20. Jack CR Jr, Bennett DA, Blennow K, Carrillo MC, Dunn B, Haeberlein SB, et al. NIA-AA Research Framework: Toward a biological definition of Alzheimer's disease. Alzheimers Dement. 2018;14(4):535-562. doi: 10.1016/j.jalz.2018.02.018
21. Nakamura A, Kaneko N, Villemagne VL, Kato T, Doecke J, Doré V, et al. High-performance plasma amyloid-β biomarkers for Alzheimer's disease. Nature. 2018;554(7691):249-254. doi:10.1038/nature25456
22. Rasmussen J, Langerman H. Alzheimer's disease - why we need early diagnosis. Degener Neurol Neuromuscul Dis. 2019; 9:123-130. doi:10.2147/DNND.S228939
23. Birks J. Cholinesterase inhibitors for Alzheimer's disease. Cochrane Database Syst Rev. 2006;(1):CD005593. doi:10.1002/14651858.CD005593
24. Hamdi NAM, Azmi NA, Sabari NHM, Harun AF, Haris MS. An insight into the use and advantages of Carbopol in topical mucoadhesive drug delivery system: A systematic review. J Pharm 2023; 3:53–65.
25. Nair AB, Chaudhary S, Shah H, Jacob S, Mewada V, Shinu P, et al. Intranasal Delivery of Darunavir-Loaded Mucoadhesive In Situ Gel: Experimental Design, In Vitro Evaluation, and Pharmacokinetic Studies. Gels 2022; 8:342. https://doi.org/10.3390/gels8060342.
26. Alkufi HK, Kassab HJ. Formulation and Evaluation of Sustained Release Sumatriptan Mucoadhesive Intranasal in-Situ Gel. Iraqi J Pharm Sci P-ISSN 1683 - 3597 E-ISSN 2521 - 3512 2019; 28:95–104. https://doi.org/10.31351/vol28iss2pp95-104.
27. Jeong S-H, Jang J-H, Lee Y-B. Drug delivery to the brain via the nasal route of administration: exploration of key targets and major consideration factors. J Pharm Investig 2023; 53:119–52. https://doi.org/10.1007/s40005-022-00589-5.
28. Kashyap K, Shukla R. Drug Delivery and Targeting to the Brain Through Nasal Route: Mechanisms, Applications and Challenges. Curr Drug Deliv 2019; 16:887–901. https://doi.org/10.2174/1567201816666191029122740.
29. Thakur R, Sharma A. An overview of mucoadhesive thermoreversible nasal gel. Asian J Pharm Res Dev 2021; 9:158–68.
30. Hard, S. A. A. A., Shivakumar, H. N., Bafail, D. A., & Moqbel Redhwan, M. A. (2024). Development of in vitro and in vivo evaluation of mucoadhesive in-situ gel for intranasal delivery of vinpocetine. Journal of Drug Targeting, 33(4), 528–545.
31. Boraste, S. V., & Patil, S. B. (2023). Formulation development and evaluation of nasal in situ gel of promethazine hydrochloride. Drug Development and Industrial Pharmacy, 50(1), 11–22.
32. Dalvi A, Ravi PR, Uppuluri CT. Design and evaluation of rufinamide nanocrystals loaded thermoresponsive nasal in situ gelling system for improved drug distribution to brain. Frontiers in Pharmacology. 2022 Oct 4; 13:943772.

Cite: Shinde Ramesh*, Bade Kanchan, Bargaje Goraksh, To Design, Develop, and Optimize a Galangin Loaded Thermosensitive In-Situ Nasal Gel for Alzheimer's Disease, Int. J. Med. Pharm. Sci., 2026, 2 (8), 246-259. https://doi.org/10.5281/zenodo.21808205